Astron. Astrophys. 324, 97–108 (1997)

ASTRONOMY
AND
ASTROPHYSICS

BD−21°3873: another yellow-symbiotic barium star⋆

V.V. Smith[1,2], K. Cunha[3], A. Jorissen[4,⋆⋆], and H.M.J. Boffin[5,⋆⋆⋆]

[1] McDonald Observatory, University of Texas, Austin, TX 78712, USA
[2] Dept. of Physics, University of Texas, El Paso, TX 79912, USA
[3] Observatório Nacional, Rua General José Cristino 77, 20921 Sao Cristovão, Rio de Janeiro, Brazil
[4] Institut d'Astronomie et d'Astrophysique, Université Libre de Bruxelles, Campus de la Plaine C.P. 226, Bd du Triomphe, B-1050 Bruxelles, Belgium
[5] Department of Earth and Planetary Sciences, Kobe University, Rokkoudai machi 1-1, Nada ku, 657 Kobe shi, Japan

Received 9 December 1996 / Accepted 20 January 1997

Abstract. An abundance analysis of the yellow symbiotic system BD−21°3873 reveals it to be a metal-poor K-giant ([Fe/H] = −1.3) which is enriched in the heavy s-process elements. In that respect, this star appears to be a twin of AG Dra, another yellow symbiotic system analyzed in a previous paper (Smith et al., 1996). The heavy-element abundance distributions of AG Dra and BD−21°3873 are almost identical, and are best reproduced by a s-process with a neutron exposure parameter of 1.2 – 1.3 mb^{-1} and a neutron density $\log N_n = 8.3$ (as derived from the Rb/Zr ratio). These two systems thus link the symbiotic stars to the binary barium and CH stars which are also s-process enriched. These binary systems, which exhibit overabundances of the heavy elements, owe their abundance peculiarities to mass transfer from thermally-pulsing asymptotic giant branch stars, which have since evolved to become white-dwarf companions of the cool stars we now view as the chemically-peculiar primaries.

The spectroscopic orbits of BD−21°3873 (derived from CORAVEL measurements) and AG Dra are similar to those of barium and CH stars. With an orbital period of 281.6 d, BD−21°3873 is one of the closest systems in these families, and its light curve indeed suggests that variations due to reflection and ellipticity effects are present. The amplitude of the ellipsoidal variations indicates that the giant must be close to filling its Roche lobe. However, no acceptable solution simultaneously satisfies the constraints from the light curve, the orbital elements and the evolutionary tracks in the framework of the standard Roche lobe geometry. We suggest that this discrepancy may be resolved by taking into account the deformation of the Roche lobe caused by the force driving the large mass loss of the giant.

Key words: binaries: symbiotic – stars: individual: BD−21°3873 – stars: abundances – stars: peculiar

1. Introduction

The families of binary systems referred to as symbiotic and barium stars (as well as their relatives the CH stars and Tc-poor S stars) share much in common in terms of their orbital characteristics and stellar components. Both types of binaries are typified by rather long orbital periods of hundreds to thousands of days and consist of cool giant components (with temperatures corresponding to spectral types G, K or M) and low-mass companions (Kenyon 1994; McClure 1984). These companions are white dwarfs (WD) in most cases (McClure & Woodsworth 1990; Brown et al. 1990; Iben & Tutukov 1996; Jorissen & Van Eck 1997). In the symbiotic binaries, the wind from the cool giant is strong, and the WD is heated by the accretion of some fraction of that wind. The wind is in turn ionized by the radiation field of the hot companion, giving rise to the visual emission lines which partially define a symbiotic system. Presumably, the barium and CH stars consist of binaries in which the cool giant does not have a mass loss rate large enough to trigger significant symbiotic activity (see Jorissen 1997). On the other hand, the cooler analogs of the barium stars, the Tc-poor S stars, display mild symbiotic activity (e.g. HD 35155 and HR 363; Brown et al. 1990; Ake et al. 1991; Jorissen et al. 1996; Jorissen 1997) due to the increased mass loss rates in this more luminous phase of giant branch evolution.

An additional characteristic that originally defined barium stars and their ilk is an overabundance of the elements heavier than iron that are synthesized by the s-process (see Käppeler et al. 1989 for a review). In an earlier paper (Smith et al. 1996 –

Send offprint requests to: A. Jorissen

⋆ Based in part on observations carried out at the European Southern Observatory (La Silla, Chile), and the Swiss telescope at the Haute-Provence Observatory (France)

⋆⋆ Research Associate, F.N.R.S., Belgium

⋆⋆⋆ Present address: Dept. of Physics and Astronomy, University of Wales, Cardiff, CF2 3YB, United Kingdom

hereafter referred to as Paper I), we demonstrated that the cool component in the yellow symbiotic system AG Dra is enriched in s-process elements, thus linking yellow symbiotic stars to barium stars. The subclass of yellow symbiotic stars is characterized by the cool component being a G or K giant rather than a M giant as in red symbiotic stars. As most normal G or K giants do not exhibit large enough mass loss rates to drive the symbiotic phenomenon, while the cooler and more luminous M giants do, the evolutionary status of the yellow symbiotics remained unclear (Schmid & Nussbaumer 1993).

In Paper I we showed that AG Dra is metal-poor ([Fe/H]= −1.3, where [X/H] = log $(N(\mathrm{X})/N(\mathrm{H}))_\star$ - log $(N(\mathrm{X})/N(\mathrm{H}))_\odot$). Because the giant branch in a metal-poor population is translated towards higher luminosities for a given $T_{\rm eff}$, it was argued that AG Dra has a larger mass loss rate than a more metal-rich giant of similar $T_{\rm eff}$. As discussed above, it is this large mass loss rate that drives the symbiotic phenomenon in a metal-poor binary such as AG Dra. By contrast, in a barium system involving a higher-metallicity yellow giant, the mass loss rate is insufficient to trigger the symbiotic activity. If these ideas are correct, abundance peculiarities similar to those of AG Dra are expected to be observed in other yellow symbiotic systems as well.

One such yellow symbiotic system is BD−21°3873. Allen (1980) assigns the spectral type G to the giant, while Schulte-Ladbeck (1988) classifies it as approximately G8 based on near-infrared spectra. The cool giant in this system has moreover been suspected to exhibit enhanced heavy-element lines (Jorissen 1989), suggestive of the barium syndrome. This suspicion is tested in this paper from a detailed abundance analysis of the cool component (Sects. 2, 3 and 4). These results are then compared to those obtained for AG Dra in Paper I.

Unlike AG Dra, BD−21°3873 does not seem to undergo outbursts, though it does exhibit photometric variations. The variations in the Strömgren y and b bands are interpreted by Niehues, Bruch & Duerbeck (1992) as due to the tidal deformation suffered by the giant star (ellipsoidal variable; Sect. 5.3). This property offers the possibility to narrow down the range of admissible parameters for the binary system, when combined with the newly derived orbital parameters presented in Sect. 5.1. Finally, it is shown in Sect. 5.4 that no consistent solution can be found satisfying the constraints from the orbital parameters, the ellipsoidal variations and the evolutionary tracks, with the usual Roche lobe geometry.

2. Observations

High-resolution spectra of BD−21°3873 were obtained on February 28, 1996 (JD 2 450 142, corresponding to phase 0.74 on Fig. 8) with the 2.1m telescope of McDonald Observatory (University of Texas). A set-up similar to the one reported in Paper I for the observation of the symbiotic star AG Dra has been used again here, namely the Cassegrain cross-dispersed Sandiford echelle spectrometer (McCarthy et al. 1993) and a Reticon 1200 x 400 pixel CCD detector providing a nominal two-pixel resolution of R = 60 000 with complete wavelength coverage from 6100 to 7900 Å.

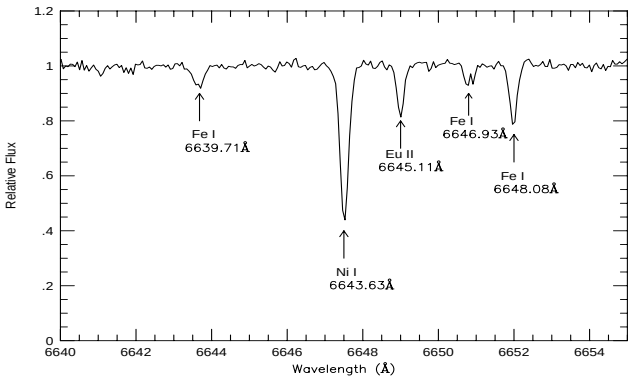

Fig. 1. The spectrum of BD−21°3873 around 6640 Å, with the strongest spectral features identified

The reduction of the spectra followed standard steps and was done with the IRAF data package. The signal-to-noise ratio achieved in the different spectral orders was typically around 100, with somewhat lower values in the far red. Fig. 1 shows a sample spectral region (around 6640 Å). We note that, at the time of the observation, the spectrum of BD−21°3873 seems generally uncontaminated by emission lines or emission continua, except for Hα and HeI λ6678Å. The broad emission features around 6825 and 7082 Å (due to OVI photons Raman scattered off HI; Schmid 1989) are not present. These features are strong in AG Dra, which is not surprising in view of the larger temperature of the ionizing source in AG Dra (170 000 K) compared to BD−21°3873 (75 000 K; Schmid & Nussbaumer 1993). Alternatively, orbital modulation may be responsible for the fact that the spectral features triggered by the ionizing source were weak or absent at the time of observation (phase 0.74, corresponding to the hot companion located behind the red giant). As shown by the lightcurve in the Strömgren c_1 index (Fig. 8, Sect. 5.3), the Balmer continuum emission is indeed weakest around phase 0.75.

3. Line selection, stellar parameters and abundances

The lines selected in this study are basically the same as in Paper I, and include lines from Fe I, Fe II Ti I, Ti II, Na I, Al I, Ca I, Sc II, V I, Ni I, Y I, Y II, Zr I, Zr II, Ba II, La II, Nd II and Eu II. The elements Ce and Hf could be measured in the spectrum of AG Dra, but not in that of BD−21°3873. Both species are only represented by a single line. In BD−21°3873, the Ce II line at λ6051.8 is obliterated by a cosmic ray, while the weak Hf I line at λ7131.8 is not measurable in our spectra of BD−21°3873 because its signal-to-noise ratio is somewhat lower in the far red, and because the line is intrinsically weaker in BD−21°3873 as compared to AG Dra.

The measured equivalent widths W_λ, the excitation potential and the adopted values of the oscillator strengths f for the selected lines are given in Tables 1 and 2. The f-values for the

Table 1. Fe I and Fe II lines used in this study

λ (Å)	Species	χ (eV)	gf	W_λ (mÅ)
6096.665	Fe I	3.98	1.660e-02	31
6151.618	Fe I	2.18	5.129e-04	106
6165.360	Fe I	4.14	3.388e-02	49
6173.336	Fe I	2.22	1.318e-03	128
6187.990	Fe I	3.94	2.692e-02	53
6252.555	Fe I	2.40	1.905e-02	178
6322.686	Fe I	2.59	3.715e-03	126
6380.743	Fe I	4.19	4.786e-02	53
6421.351	Fe I	2.28	9.772e-03	179
6430.846	Fe I	2.18	9.772e-03	190
6593.871	Fe I	2.44	3.802e-03	141
6597.561	Fe I	4.80	1.202e-01	30
6609.110	Fe I	2.56	2.042e-03	129
6733.151	Fe I	4.64	3.715e-02	17
6750.153	Fe I	2.42	2.399e-03	134
6820.372	Fe I	4.64	6.761e-02	30
6858.150	Fe I	4.61	1.175e-01	35
6149.246	Fe II	3.89	1.905e-03	20
6416.921	Fe II	3.89	2.089e-03	31
6432.682	Fe II	2.89	2.630e-04	40

Fe lines listed in Table 1 are taken from the recent critical assessment of laboratory results by Lambert et al. (1996). The sources of the f-values for the other lines are listed in Table 2. A discussion of the f-values employed in the calculations and of the corresponding uncertainties has been presented in Paper I and will not be repeated here.

Since the $H-K$ and $J-K$ colors of BD−21°3873 and AG Dra are almost identical ($J-K$ = 0.91 and 0.94, $H-K$ = 0.16 and 0.18 for AG Dra and BD−21°3873, respectively; Kenyon 1988), similar effective temperatures may be expected for these two stars. The atmospheric parameters derived in Paper I for AG Dra have thus been adopted as starting values for BD−21°3873. A fine tuning of these initial values was performed using the same spectroscopic methods as in Paper I for AG Dra, with model atmospheres from Bell et al. (1976) (starting with [M/H]= −1.5 models and iterating to be consistent with the final derived [Fe/H] value). The adopted effective temperature is the one ensuring that the Fe abundances derived from the various lines do not depend upon their excitation potential, while the agreement between the Fe I and Fe II average abundances fixes $\log g$. The microturbulent velocity ξ was determined from the zero slope of the Fe abundances with the reduced equivalent widths W_λ/λ. The parameters derived in this manner for BD−21°3873 are [Fe/H]= −1.34, $T_{\rm eff}$ = 4300 K, $\log g$ = 1.0 and ξ = 2.15 km s^{-1}, to be compared with [Fe/H]= −1.3, $T_{\rm eff}$ = 4300 K, $\log g$ = 1.6 and ξ = 2.25 km s^{-1} for AG Dra. Our detailed spectroscopic analyses thus yield identical effective temperatures for BD−21°3873 and AG Dra, as already suspected from the similarity of their near-infrared colors. The surface gravity appears to be somewhat lower in BD−21°3873

Table 2. Other lines studied

λ (Å)	Species	χ (eV)	gf	Ref	W_λ (mÅ)
6126.220	Ti I	1.05	3.802e-02	B83	106
6258.100	Ti I	1.44	4.467e-01	B86	135
6261.100	Ti I	1.43	3.311e-01	B86	149
6312.240	Ti I	1.46	2.805e-02	B86	52
6336.100	Ti I	1.44	1.807e-02	B86	48
6599.110	Ti I	0.90	8.222e-03	B83	70
6743.120	Ti I	0.90	2.344e-02	FMW88	103
6606.970	Ti II	2.06	1.622e-03	FMW88	37
6154.200	Na I	2.10	2.951e-02	LL78	18
6160.800	Na I	2.10	5.888e-02	LL78	18
6696.030	Al I	3.14	4.786e-02	LL78	23
6698.700	Al I	3.14	2.399e-02	LL78	14
6161.300	Ca I	2.52	9.333e-02	WM80	85
6166.440	Ca I	2.52	7.244e-02	S86	95
6169.040	Ca I	2.52	1.585e-01	DS91	116
6169.560	Ca I	2.53	3.311e-01	DS91	124
6439.080	Ca I	2.51	2.950e+00	WM80	189
6455.600	Ca I	2.51	4.571e-02	S86	80
6508.840	Ca I	2.51	3.890e-03	WM80	16
6245.620	Sc II	1.51	9.550e-02	YA89	77
6604.600	Sc II	1.36	4.900e-02	LD89	75
6357.300	V I	1.85	1.230e-01	FMW88	16
6785.000	V I	1.05	1.413e-02	FMW88	14
6327.600	Ni I	1.68	7.709e-04	FMW88	98
6482.800	Ni I	1.94	2.344e-03	FMW88	100
6532.890	Ni I	1.94	4.074e-04	FMW88	50
6586.330	Ni I	1.95	1.549e-03	FMW88	84
6643.640	Ni I	1.68	5.012e-03	FMW88	163
6767.770	Ni I	1.83	6.761e-03	FMW88	149
6772.360	Ni I	3.66	1.047e-01	FMW88	49
6222.610	Y I	0.00	2.042e-02	H82	4
6435.000	Y I	0.07	1.510e-01	H82	20
6795.410	Y II	1.74	5.012e-02	S	14
6127.460	Zr I	0.15	8.710e-02	B81	49
6134.570	Zr I	0.00	5.248e-02	B81	38
6114.800	Zr II	1.66	1.778e-02	S	11
6496.900	Ba II	0.60	4.170e-01	WM80	190
6390.480	La II	0.32	2.750e-02	S	36
6774.330	La II	0.12	1.778e-02	S	46
6637.190	Nd II	1.45	8.913e-02	S	7
6645.110	Eu II	1.37	1.580e+00	B82	48

References to Table 2: B81: Biémont et al. (1981); B82: Biémont et al. (1982); B83: Blackwell et al. (1983); B86: Blackwell et al. (1986); DS91: Drake & Smith (1991); H82: Hannaford et al. (1982); LD89: Lawler & Dakin (1989); LL78: Lambert & Luck (1978); FMW88: Fuhr, Martin & Wiese (1988); S: Solar gf-values (Paper I); S86: Smith et al. (1986); WM80: Wiese & Martin (1980); YA89: Youssef & Amer (1989)

Table 3. Derived Abundances

Species	n	$\log \epsilon^a$	Technique^b	[X/Fe]
Fe I	16	6.17 ± 0.06	EQW	–
Fe II	3	6.21 ± 0.13	EQW	–
[O I]	1	8.06	SS	+0.46
Na I	2	4.78	EQW	−0.22
Al I	2	5.11	EQW	−0.03
Ca I	7	5.25±0.12	EQW	+0.22
Sc II	2	1.94	EQW	+0.17
Ti I	7	4.14±0.11	EQW	+0.48
Ti II	1	4.21	EQW	+0.55
V I	2	3.22	EQW	+0.55
Ni I	7	5.01±0.09	EQW	+0.09
Rb I	1	1.75	SS	+0.50
Y I	2	1.21	EQW	+0.30
Y II	1	1.19	EQW	+0.28
Zr I	2	1.88	EQW	+0.61
Zr II	1	1.91	EQW	+0.64
Ba II	1	1.10	EQW	+0.30
La II	2	0.38	EQW	+0.49
Nd II	1	0.95	EQW	+0.78
Eu II	1	-0.20	SS	+0.64

[a] Abundances in the scale $\log \epsilon$(H) = 12
[b] EQW = Equivalent Width; SS = Spectrum Synthesis

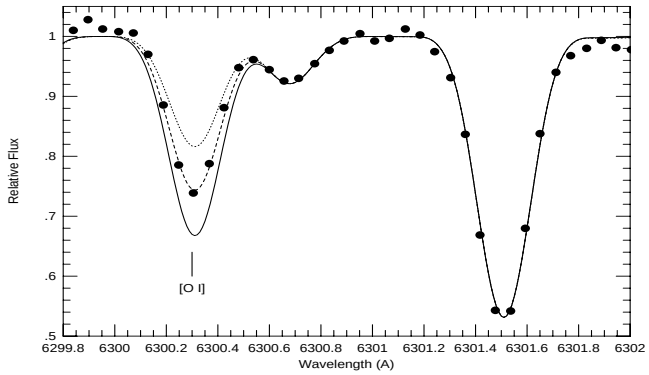

Fig. 2. Comparison of the observed (dots) and synthetic spectra near the [OI] λ6300 line. The solid, dashed and dotted lines correspond to O abundances of $\log \epsilon$(O) = 8.26, 8.06 and 7.86, respectively [in the scale $\log \epsilon$(H) = 12]

as compared to AG Dra. The derived temperature and gravity are certainly consistent with Schulte-Ladbeck's (1988) classification of BD−21°3873 as a late G-giant, especially since it is somewhat metal-poor.

The obtained standard deviation of 0.06 dex on the Fe I abundance (Table 3) illustrates the quality of the equivalent widths and model atmosphere analysis (as discussed in Paper I, the uncertainties in the Fe I laboratory gf-values alone are about 0.05 dex). The low metallicity of BD−21°3873 derived from our detailed abundance analysis coupled with its systemic radial velocity of +204 km s^{-1} (Sect. 5.1 and Table 6) clearly tags this symbiotic system as a member of the galactic halo population. Using the derived $T_{\rm eff}$ and $\log g$ values, and a reasonable estimate of the stellar mass (0.9 $M_\odot$), one finds $\log(L/L_\odot)$ = 2.89 or $M_{\rm bol}$ = −2.5 (A more accurate calculation, using the constraints provided by the ellipsoidal light variations, will be presented in Sect. 5.4). The cool component of BD−21°3873 is thus a rather luminous giant. The implications of this fact will be discussed in Sect. 5.4.

The program MOOG (Sneden 1973) has been used to derive the abundances from the measured equivalent widths for all species except [OI], Rb I and Eu II, for which spectrum synthesis is required due to important blending and/or hyperfine splitting. Figs. 2 and 3 compare the synthetic and observed spectra near the [OI] λ6300 and Rb I λ7800 lines, respectively. These figures illustrate both the quality of the data and the agreement obtained between synthetic and observed spectra. Note that the spectrum has a higher signal-to-noise ratio in the region near the [OI] line than near the Rb I line. However, it is clear from Fig. 3 that the Rb I line is detectable and an abundance can be derived from this feature. Our abundance results are listed in Table 3 along with their standard deviations due to the line-to-line scatter. The uncertainties introduced by the errors in the stellar parameters have been studied in Paper I in relation with AG Dra, but are expected to be similar for BD−21°3873 given the similarities in the atmospheric parameters of the two stars. We thus refer to Paper I for a detailed discussion of these uncertainties, which are generally of the order of 0.2 dex for the heavy elements (0.5 dex for Ba II, because the only available lines are strong and thus sensitive to microturbulence).

4. Abundance pattern

As seen on Fig. 4, the abundance pattern obtained for BD−21°3873 very closely follows the one found for AG Dra in Paper I. Both stars are characterized by moderate enhancements of the α-elements with respect to Fe, with [O/Fe]=+0.46, [Ca/Fe]=+0.22, and [Ti/Fe]=+0.50. On the contrary, Na, Al, Sc and Ni all have roughly solar or subsolar abundance ratios relative to Fe. These trends are exactly those expected in low-metallicity stars as a result of the chemical evolution of the Galaxy (see e.g. Wheeler et al. 1989). Only V deviates from these expectations in being overabundant in both stars, but as already emphasized by Wheeler et al. (1989), the lack of accurate accounting for possible hyperfine structure of the V lines hampers current abundance determinations for that element.

Inspection of Fig. 4 also reveals that BD−21°3873 shows a general overabundance of the elements heavier than Rb and synthesized by neutron captures. The available abundances in low-metallicity dwarf stars (e.g. Magain 1989; Zhao & Magain 1990; Edvardsson et al. 1993) indicate that the chemical evolution of the Galaxy cannot be responsible for the overabundances observed in BD−21°3873. In dwarf halo stars with metallicities [Fe/H] ~ -1.5, the neutron-capture elements Y, Ba and La have solar abundance ratios relative to Fe (Gilroy et al. 1988; Magain 1989). As far as Nd is concerned, the absence of any trend in Edvardsson et al. (1993) data for disk dwarfs (i.e. [Nd/Fe] = 0

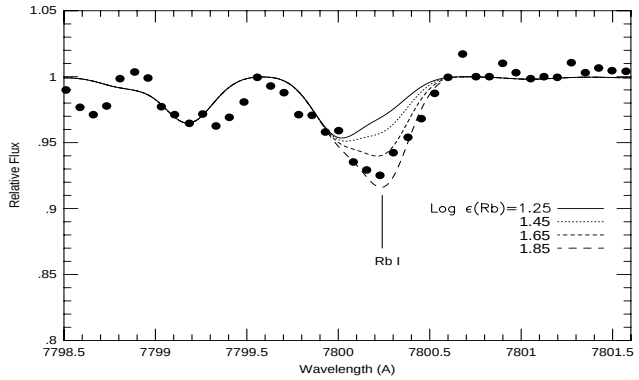

Fig. 3. Same as Fig. 2 for the region near the Rb I λ7800 line

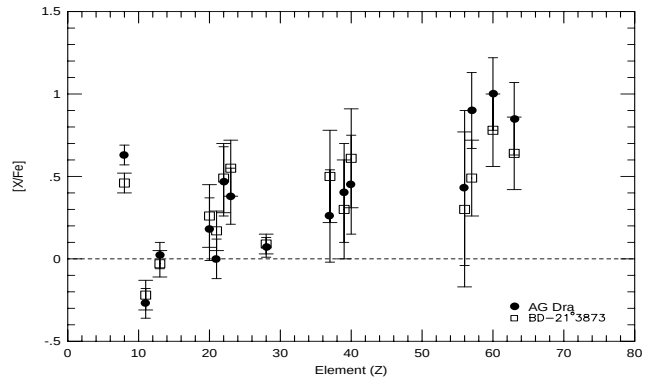

Fig. 4. The [X/Fe] abundance ratios in BD−21°3873 (open squares) and AG Dra (black dots) relative to solar (where [X/Fe] $\equiv \log\epsilon(\mathrm{X})/\epsilon(\mathrm{Fe})_* - \log\epsilon(\mathrm{X})/\epsilon(\mathrm{Fe})_\odot$)

down to [Fe/H]= −1) suggests that, as for the above-mentioned elements, the Nd/Fe ratio will remain solar down to the metallicity [Fe/H]= −1.3 of BD−21°3873. This result is confirmed by Luck & Bond (1985) for a sample of halo giants.

On the contrary, the Eu/Fe and Zr/Fe ratios do not remain solar at metallicities [Fe/H]~ -1.5. A trend of increasing Zr/Fe with decreasing [Fe/H] in disk stars is barely noticeable in the data of Edvardsson et al. (1993), while Zhao & Magain (1991) find [Zr/Fe]$\sim$ +0.2 in dwarf halo stars with metallicities [Fe/H] ~ -1.5 similar to that of BD−21°3873. Similarly, [Eu/Fe] increases from 0 at solar metallicity to about 0.4 at [Fe/H]= −1 in the disk stars observed by Woolf et al. (1995), while Magain (1989) reports [Eu/Fe] $\sim$ +0.5 in dwarf halo stars with [Fe/H] ~ -1.5.

The overabundances of neutron-capture elements observed in BD−21°3873 are much larger than those (if any) expected from the chemical evolution of the Galaxy, so that our observations indicate that BD−21°3873 is yet another example of a yellow symbiotic barium star. As in the barium stars (see e.g. Jorissen & Boffin 1992), the chemical peculiarities observed in BD−21°3873 are thus likely to result from the accretion of s-process-rich material ejected by the companion in a former state of the binary system.

Table 4. Comparison between the observed heavy-element abundances in BD−21°3873 and parametrized s-process model predictions. The columns labeled $\log\epsilon_{\rm obs}$ and $\log\epsilon_{\rm i}$ contain the observed abundances and the solar abundances scaled down to metallicity [Fe/H]= −1.3, respectively (in the scale $\log\epsilon$(H) = 12). The columns labeled $\log\epsilon'_s$ contain the abundances in the neutron-irradiated matter, as inferred from the observations and as predicted by a model with τ = 1.2 mb^{-1} and $\log N_n$ = 8.3. See Paper I for details

Species	$\log\epsilon_{\rm obs}$	$\log\epsilon_i$	$\log\epsilon'_s$	
			observed	model
Rb	1.75	1.26	1.58	0.46
Y	1.20	0.91	0.89	0.84
Zr	1.89	1.27	1.77	1.40
Ba	1.10	0.80	0.80	1.71
La	0.38	-0.11	0.21	0.59
Nd	0.95	0.17	0.87	1.44
Eu	-0.20	-0.34	-0.76	-1.07

The neutron exposure and neutron density characterizing the s-process episode in the former AGB companion (now a WD) can be derived from the observed overabundances according to the method outlined in Paper I. The abundances ϵ'_s in the accreted material are first derived using Eqs. (3) and (4) of Paper I; they are listed in Table 4. These abundances are then compared to the predictions of s-process nucleosynthesis calculations as provided by Malaney (1987). The neutron exposure τ and neutron density $N_{\rm n}$ yielding the best fit [as expressed by Eq. (5) of Paper I] are then retained. Not surprisingly given the similarities in the abundance distributions of AG Dra and BD−21°3873, the best fit for BD−21°3873 is obtained for a value of τ = 1.2 mb^{-1}, very similar to that (1.3 mb^{-1}) found for AG Dra. Both of these values are higher than the one characterizing the solar system material (Käppeler et al. 1989) and are similar to what Vanture (1992a) found for the metal-poor CH stars.

The derived Rb/Zr abundance ratio in the s-processed material is used next to estimate the neutron density. A value of [Rb/Zr]= $\log\epsilon'_s/\epsilon_i$(Rb) − $\log\epsilon'_s/\epsilon_i$(Zr) = −0.18 is derived for BD−21°3873 (Table 4), corresponding to $\log N_{\rm n}$ = 8.30 according to the predictions of Malaney (1987) and Malaney & Lambert (1988). This value of [Rb/Zr] is derived by using the solar photospheric Rb abundance of $\log\epsilon$ = 2.60, as opposed to the meteoritic value of 2.41 (Anders & Grevesse 1989). Within the uncertainties, the neutron densities and metallicities of AG Dra and BD−21°3873 are thus identical. These results strengthen the trend of increasing neutron densities with decreasing metallicities inferred in Paper I (Fig. 7) from AG Dra and the barium stars analyzed by Tomkin & Lambert (1983, 1986), Smith & Lambert (1984), and Malaney & Lambert (1988). Such a trend is indeed expected if ^{13}C(α,n)^{16}O is the neutron source (Clayton 1988). A least-square fit to the barium star data together with AG Dra and BD−21°3873 yields a slope of −1.0 for a linear relation between $\log N_{\rm n}$ and [Fe/H] (with a correlation coeffi-

cient of r = 0.98), identical to the simple theoretical value of −1 predicted by Clayton's argument (see Paper I). We note that the value of [Rb/Zr] for AG Dra is -0.33 and that this point is misplotted in Fig. 7 of our Paper I.

Relative C, N and O abundances have been derived for the BD−21°3873 and AG Dra systems by Schmid & Nussbaumer (1993). These authors point out that both of these objects have rather low C/O ratios of 0.28 and 0.17, respectively. As the s-process elements are believed to be synthesized during the He-burning thermal pulses on the AGB, freshly synthesized heavy elements *and* ^{12}C should be dredged to the surface of an AGB star altogether. Thus the rather low C/O ratios derived by Schmid & Nussbaumer might at first seem incompatible with this standard scenario for s-process production. However, combining these C/O ratios with our absolute O abundances (that appear to be typical of halo stars), we estimate the carbon content of AG Dra and BD−21°3873 to be [C/Fe]= +0.22 and +0.29, respectively. Carbon is thus clearly overabundant in these two symbiotic systems, especially considering the fact that [C/Fe] = 0 in dwarf halo stars (Wheeler et al. 1989). The first dredge-up occurring at the base of the giant branch is expected to reduce the relative carbon content in the envelope of a giant star (e.g. Lambert & Ries 1981), thus reinforcing the significance of the carbon overabundances observed in AG Dra and BD−21°3873. Indeed, in a plot of s-process versus carbon overabundances (Fig. 11 of Smith & Lambert 1990), these two symbiotic systems fall close to the relation defined by the barium and S stars.

In conclusion, BD−21°3873 and AG Dra are identical twins in terms of metallicities, carbon overabundances, s-process abundance distributions (as defined by the neutron exposure), and s-process neutron densities (as inferred from the Rb/Zr ratio). Both stars exhibit the barium syndrome, and should thus somehow be related to the CH stars, the low-metallicity relatives of barium stars (McClure 1984), as discussed in Sect. 5.2.

5. Binary parameters and evolutionary status

5.1. Orbital elements

The radial velocity monitoring of BD−21°3873 has been performed by means of the CORAVEL spectrovelocimeters (Baranne et al. 1979) installed on the 1.0 m Swiss telescope at the Haute-Provence Observatory (France) and on the Danish 1.5 m telescope at the European Southern Observatory (ESO, La Silla, Chile). Individual radial velocity measurements for BD−21°3873 are listed in Table 5. All radial velocities are in the system defined by the faint IAU standards as given by Mayor & Maurice (1985). The orbital parameters listed in Table 6 were obtained by forcing the orbit to be circular. If the eccentricity is left free, a solution with e = 0.07 ± 0.02 (and 0.62 km s^{-1} residuals) is found, not significant at the 5% level according to Lucy & Sweeney's (1971) criterion.

Finally, it has to be remarked that the systemic radial velocity of 204 km s^{-1} clearly tags BD−21°3873 as a halo member.

Table 5. Individual radial velocity measurements of BD−21°3873. Columns 1 and 2 provide the date and the heliocentric Julian Date, respectively. Column 3 lists the radial velocity measurements with the corresponding uncertainties given in column 4. The $O-C$ ('observed-computed') values relative to the orbital solution listed in Table 6 are given in column 5. Column 6 is a four-character code for the observer, as listed in Table 3 of Duquennoy, Mayor & Halbwachs (1991)

Date	HJD	RV	ϵ_1	$O-C$	Observers
da-mo-yr	−2440000	km s^{-1}	km s^{-1}	km s^{-1}	
27-06-91	8435.517	199.23	0.61	−0.04	DUQU
18-07-91	8456.499	204.45	0.36	−0.31	MERM
15-01-92	8637.869	196.39	0.58	0.25	DUQU
24-03-92	8706.915	197.05	0.44	0.17	JORI
15-04-92	8728.827	201.76	0.33	−0.33	LIND
09-05-92	8752.516	209.84	0.42	1.19	DUQU
22-05-92	8765.602	210.91	0.36	−0.17	MAYO
15-06-92	8789.696	213.25	0.48	−0.78	ANDE
06-08-92	8841.482	210.30	0.37	−0.48	JORI
07-03-93	9054.845	212.14	0.35	−0.12	JORI
20-04-93	9098.552	214.67	0.44	0.55	DUQU
21-02-94	9405.884	211.34	0.43	0.55	WAEL
06-04-94	9449.529	202.34	0.74	−0.56	PERN
20-06-94	9524.706	193.40	0.43	−0.08	NORT
20-03-95	9797.851	193.44	0.37	0.03	UDRY

Table 6. Orbital parameters of BD−21°3873, derived from the CORAVEL measurements listed in Table 5 by imposing a zero eccentricity. All symbols have their usual meaning, $\overline{\epsilon_1}$ being the mean uncertainty on one measurement

P (d)	281.6	±1.2
T (JD)	2 449 087.3	±1.6
e	0.00	
V_0 (km s^{-1})	203.9	±0.2
ω	–	
K_1 (km s^{-1})	10.6	±0.3
$A_1 \sin i$ (AU)	0.276	±0.008
$f(M)$ (M$_\odot$)	0.035	±0.003
N	15	
σ_{O-C} (km s^{-1})	0.79	
$\overline{\epsilon_1}$ (km s^{-1})	0.41	

5.2. Yellow symbiotics vs CH stars

As concluded in Sect. 4, BD−21°3873 adds to the sample of yellow symbiotics like AG Dra (Paper I), UKS-Ce1 and S32 (Schmid 1994) exhibiting the barium syndrome. The present section therefore compares various properties of barium stars, CH stars and yellow symbiotics.

Fig. 6 compares the orbital period distributions of these three families. The samples of barium and CH systems are from Jorissen & Van Eck (1997) and McClure & Woodsworth (1990), respectively. The sample of yellow symbiotic stars includes BD−21°3873, AG Dra (Paper I), TX CVn (Kenyon & Garcia 1989) and LT Del (= He2- 467; Arkhipova & Noskova 1988, Munari & Buson 1992). Yellow symbiotic stars clearly cluster

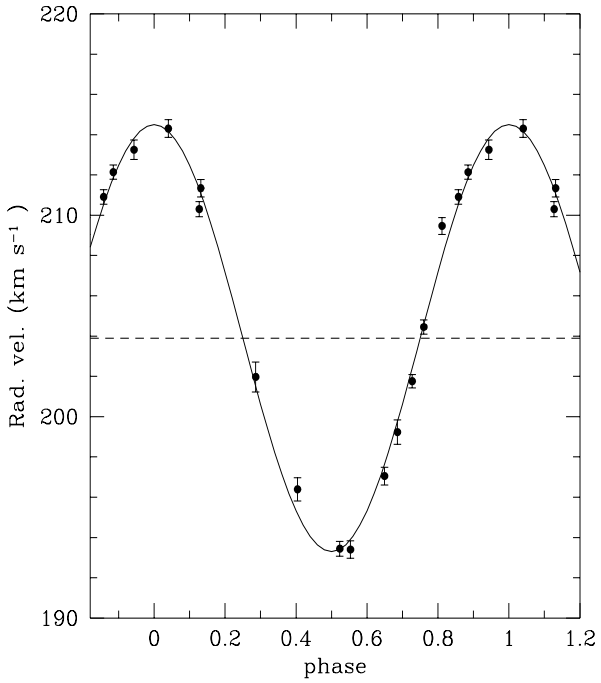

Fig. 5. Orbital phase diagram of BD−21°3873

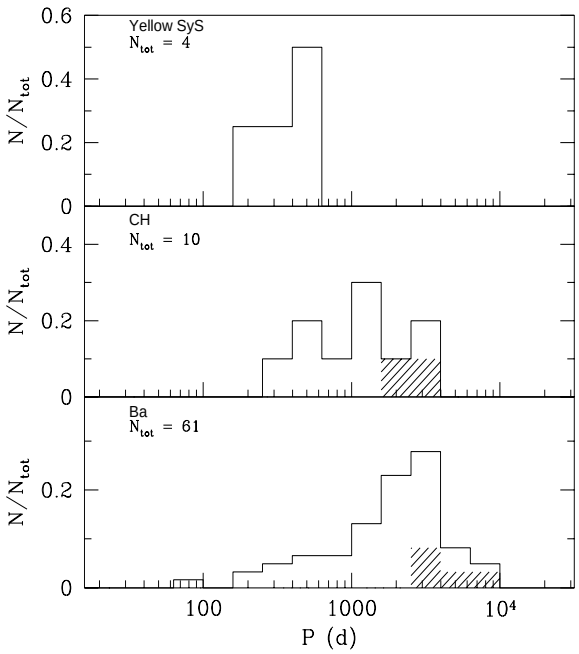

Fig. 6. Distribution of the orbital periods of barium stars (bottom panel, from Jorissen & Van Eck 1997), CH stars (middle panel, from McClure & Woodsworth 1990) and yellow symbiotic stars (top panel; see text for references), with bins of width 0.2 in $\log P$. The shaded region corresponds to systems with only a lower limit available on the period

at the short-period end of the barium and CH distributions, but this difference would need to be confirmed on a larger sample of yellow symbiotic stars.

Fig. 7 compares effective temperatures and metallicities for CH stars (from Vanture 1992b) and yellow symbiotic-barium stars. It is clearly apparent that CH stars are, on the average, hotter than the yellow symbiotic-barium stars, and therefore also probably somewhat less luminous (because $\mathrm{d}T_{\rm eff}/\mathrm{d}L < 0$ on the giant branch, and assuming that the two families involve stars of approximately the same mass). Assuming that Reimers' (1975) mass loss law (stating that $\dot{M} \propto L$) applies to these systems, CH stars should then lose mass at a lower rate than yellow symbiotics, explaining why the former do not exhibit symbiotic activity. The longer orbital periods found among CH stars (Fig. 6) are probably another reason for their lack of symbiotic activity. The accretion rate by the compact companion is a key ingredient for triggering the symbiotic activity (e.g. Iben & Tutukov 1996). Since this accretion rate decreases with increasing orbital separation (all other parameters being equal), for a given mass loss rate of the giant component, short-period systems will thus more easily exhibit symbiotic activity. A more detailed comparison of symbiotic stars and peculiar red-giant stars can be found in Jorissen (1997).

5.3. Light curve

The symbiotic star BD−21°3873 has been extensively monitored in the framework of the Long-Term Photometry of Variables (LTPV) program carried out at ESO (Sterken 1983). In the interval JD 2 446 304 (September 1985) to 2 449 593 (September 1994), 53 observations were performed in the Strömgren $uvby$ bands using HD 126036 (G2/G3V) and HD 124122 (G8III/IV) as comparison stars. Individual measurements are listed in the LTPV catalogues (Sterken et al. 1995a,b and references therein). Fig. 8 presents the $uvby$ light curves phased with the orbital period listed in Table 6 and including only measurements performed on the Strömgren Automatic Telescope (SAT) and expressed in the natural SAT photometric system (see Sterken et al. 1995a for details). The y and b magnitudes appear to vary with a period $P_{\rm orb}/2$, whereas the u and v magnitudes, as well as the color indices, vary in phase with the orbit.

The average value of the $c_1[\equiv (u-v)-(v-b)]$ index (-0.5) is much smaller than that of normal K giants (0.4; Olsen 1984, Jorissen et al. 1997), thus reflecting Balmer continuum emission, as also seen on Allen's (1984) spectrum of BD−21°3873. The maximum negative c_1 value is observed at the inferior conjunction of the companion, when the hemisphere of the giant illuminated by the companion faces the observer. A similar orbital modulation, though with a somewhat smaller amplitude, is observed in the v band as well. Such an orbital modulation with an amplitude increasing towards shorter wavelengths is observed in many symbiotic systems (e.g. Arkhipova & Noskova 1985, 1988; Munari 1989; Munari & Buson 1992; Kolotilov et al. 1995; Schild et al. 1996) and is ascribed to the reflection (or heating) effect (e.g. Morris & Naftilan 1993; Proga et al. 1996). The temperature of the hot companion in BD−21°3873 is estimated to be 75 000 K from the HeII equivalent width (Schmid & Nussbaumer 1993). As stressed by Munari (1989) and Schild et al. (1996), the sinusoidal shape of the light curves for all

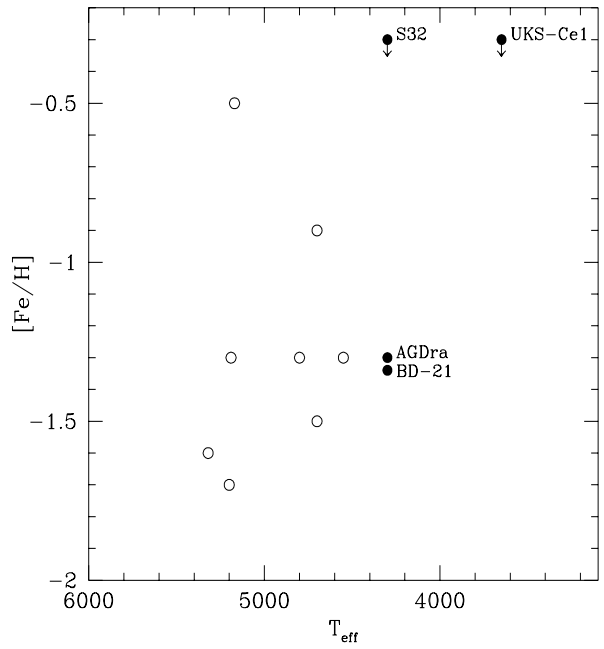

Fig. 7. Comparison of the metallicities [Fe/H] and $T_{\rm eff}$ of CH stars (open circles, from Vanture 1992b) and yellow symbiotic-barium stars (filled circles). Metallicities for S32 and UKS-Ce1 were not provided by Schmid (1994)

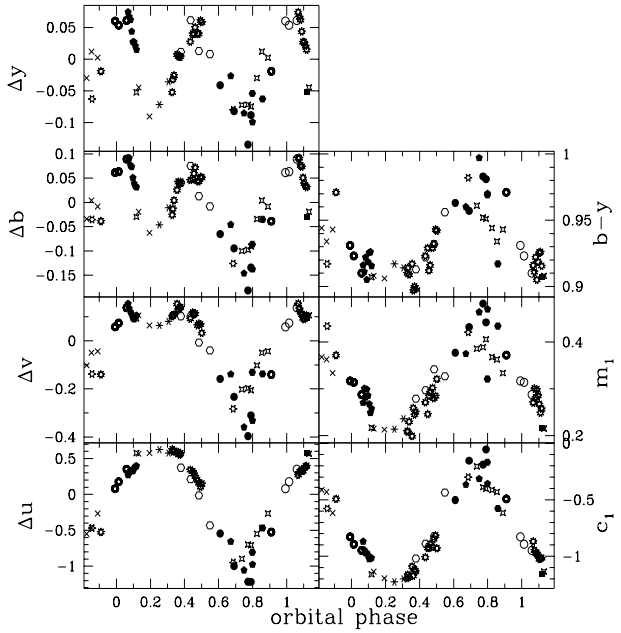

Fig. 8. The lightcurve of BD−21°3873 in the four $uvby$ bands (from bottom to top, left panels), and the $b-y$, m_1 and c_1 color indices (from top to bottom, right panels). All data have been phased with the 281.6 d orbital period, with phase 0.25 corresponding to the maximum distance of the giant from the Sun (inferior conjunction of the companion). The $uvby$ lightcurves are differential [i.e. $P-(A+B)/2$, where P stands for BD−21°3873 and A and B for the two comparison stars]; their zero point corresponds to the average value over the whole monitoring. Different symbols refer to different orbital cycles. Brightness increases towards the top. The larger scatter observed in the u and v light curves around phase 0.75 is due to the fact that the star is much fainter in the violet at that phase

these systems, including BD−21°3873 (Fig. 8), suggests that the symbiotic nebulosity responsible for the Balmer continuum emission must be closely confined to the immediate neighbourhood of the red giant.

The double-sine patterns observed in the y band and, to a lesser extent, in the b band indicate that variations of a different nature are superimposed on the reflection effect. Niehues et al. (1992) already suggested that the ellipticity effect (due to the geometrical deformation of the giant star by the gravitational potential of its companion) is most likely at the origin of the variations dominating the b and y bands. In fact, ellipsoidal variations are almost grey (except for the small color effect introduced by the wavelength-dependence of the limb- and gravity-darkening coefficients; Morris 1985, Morris & Naftilan 1993). This is indeed the case for BD−21°3873, since the secondary minimum centered on phase 0.25 has a depth of about 0.15 mag in all three vby bands (and is not detectable anymore in the u band where the reflection effect largely dominates).

5.4. Combined photometric and spectroscopic solution

The existence of ellipsoidal variations offers the possibility to narrow down the range of admissible parameters for the binary system, by combining the constraints provided by the lightcurve, the spectroscopic orbital elements and evolutionary considerations. The barium nature of the giant in BD−21°3873 imposes that the compact companion be a carbon-oxygen WD. In order to synthesize the s-process elements which polluted the barium star during a former mass-transfer episode, the AGB progenitor of the present WD must clearly have gone through the TP-AGB phase. According to Lattanzio (1986), the mass of the CO core at the first thermal pulse amounts to 0.44 $M_\odot$ in a $Z = 0.001, Y = 0.02, M = 1$ $M_\odot$ star, and it increases rapidly with M, reaching 0.72 $M_\odot$ for $M = 3.0$ $M_\odot$. Thus a further constraint may be expressed as $M_2 \gtrsim 0.4$ $M_\odot$(where M_2 designates the current WD mass). Niehues et al. (1992) found that a reasonably good fit to the Strömgren y and b lightcurves could be obtained for an orbital inclination $i = 68°$ and a mass ratio $q = M_1/M_2 = 1.8$ (where M_1 is the red-giant mass), using the standard Wilson & Devinney (1971) code. When combined with the spectroscopic mass function listed in Table 6, that particular photometric solution implies $M_1 = 0.58$ $M_\odot$ and $M_2 = 0.32$ $M_\odot$, and is thus incompatible with the above evolutionary constraint.

In fact, solutions fitting the y lightcurve, and satisfying the evolutionary constraint on M_2 expressed above as well as the spectroscopic orbital elements, may be searched using the method outlined by Hall (1990) and Jorissen et al. (1995). In particular, given $A_1 \sin i$, $f(M)$ and Δy (the peak-to-peak amplitude of the light variations in the y band), Eq. (1) of Jorissen et al. (1995) provides R_1, the radius of the red giant, as a func-

tion of the free parameters M_2 and Q, or equivalently, M_2 and $\sin i$, where $Q \equiv f(M)/\sin^3 i \equiv M_2^3/(M_1 + M_2)^2$. The mass M_1 of the giant is then extracted from the previous relation. The radius R_1 may then be converted into the corresponding bolometric magnitude using the relation

$$M_{\rm bol} = 42.26 - 5\log(R_1/{\rm R}_\odot) - 10\log T_{\rm eff}, \quad (1)$$

where $T_{\rm eff}$ = 4300 K for BD−21°3873 as derived in Sect. 3. The solutions may then be represented in a ($M_{\rm bol}$, M_1) diagram and compared to the predictions of evolutionary calculations for the given $T_{\rm eff}$ and metallicity.

The method outlined above implicitly assumes that the observed variations directly reflect the deformation of the giant star, or in other words, that (a) the companion star does not contribute to the system light in the y band, (b) the companion does not contribute its own ellipsoidal variations, and (c) the reflection effect is negligible in the y band. The last assumption is validated by the almost equal depth of the minima observed in the y lightcurve (Fig. 8). In order to check assumption (a), the companion's continuum in the y band may be evaluated from its continuum flux at 150 nm ($\sim 10^{-12}$ erg cm^{-2} s^{-1} nm^{-1}; Schmid & Nussbaumer 1993) and from the assumption that the companion radiates as a black body. The slope of the continuum in the IUE SWP spectrum presented by Schmid & Nussbaumer (1993) is consistent with that of an unreddened hot black body. A flux of 9.4 10^{-15} erg cm^{-2} s^{-1} nm^{-1} at λ = 550 nm is then derived for T = 75 000 K. The corresponding magnitude $y \sim 16.5$ (derived from the flux – magnitude calibration of Straizys & Kurilienė 1975) is much fainter than the magnitude of the red giant (y = 10.9), thus validating assumption (a). Assumption (b) automatically follows if (a) is satisfied. With these assumptions, Δy = 0.14 mag for BD−21°3873 (Fig. 8).

Fig. 9 compares $M_{\rm bol}$ derived from the dynamical solution (ellipsoidal variations + spectroscopic orbit) through Eq. (1) with the Geneva evolutionary tracks (Schaller et al. 1992; Charbonnel et al. 1996) for Z = 0.001 ([Fe/H] = −1.3). There appears to be no solutions matching the evolutionary tracks, since the bolometric magnitude derived from the dynamical solution is always at least 1 mag brighter. The fact that BD−21°3873 is a halo giant star suggests $0.8 \lesssim M_1({\rm M}_\odot) \lesssim 1.0$, which in turn implies $M_2 \lesssim 0.45$ M$_\odot$ from Fig. 9, just satisfying the requirement that the WD progenitor went through the TP-AGB phase (i.e. $M_2 \gtrsim 0.40$ M$_\odot$). In fact, such typical values of M_1 = 0.9 M$_\odot$ and M_2 = 0.45 M$_\odot$ combined with the orbital elements yield a Roche radius $R_{\rm R}$ of the order of 90 R$_\odot$ (as derived from the usual restricted three-body equipotentials; e.g. Kopal 1959), whereas the stellar radius consistent with the evolutionary tracks amounts to R = 37 R$_\odot$. The corresponding filling factor $R/R_{\rm R}$ = 0.4 is much too small to account for the observed amplitude of the ellipsoidal variations ($\Delta y \sim 0.14$ mag). That amplitude is in fact close to the maximum value that may be achieved in such circumstances (see e.g. Fig. 1 of Morris 1985), indicating that the giant star must be very close to filling its Roche lobe.

This discrepancy may be interpreted in various ways: (i) the observed variations are not solely due to the geometrical deformation of the giant star; or (ii) the evolutionary tracks used in Fig. 9 incorrectly reproduce the position of BD−21°3873 in the Hertzsprung-Russell diagram; or (iii) the Roche radius is smaller than the usual value derived from the restricted three-body equipotentials.

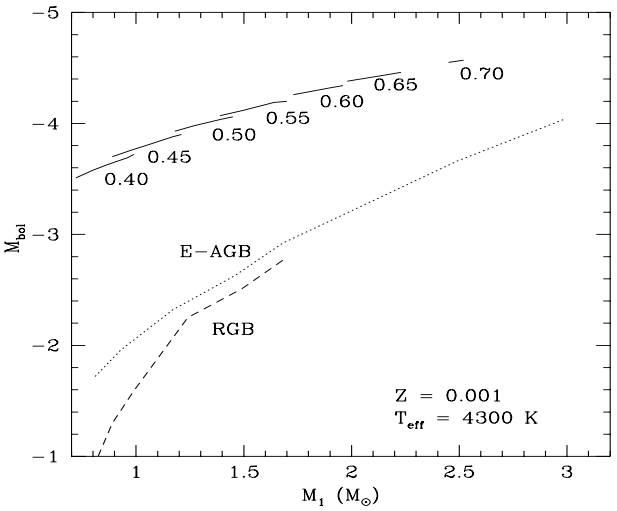

Fig. 9. Range of (M_1, M_2, $M_{\rm bol}$) values compatible with the ellipsoidal variations and the spectroscopic orbital elements (solid lines, labelled by M_2 expressed in M$_\odot$). The left boundary of each segment corresponds to the star filling its Roche-lobe, whereas the right limit is set by $\sin i \leq 1$. In all cases, the filling factor is larger than 0.95. The dashed and dotted lines correspond to the loci of Z = 0.001 stars of mass M_1 with $T_{\rm eff}$ = 4300 K on the RGB and E-AGB, respectively, according to Schaller et al. (1992) and Charbonnel et al. (1996)

Statement (i) would imply that the above assumptions (a) to (c) are not valid. Since they appear however plausible when the companion's flux in the optical is estimated in the framework of the black body approximation, progress towards a more satisfactory solution in the context of statement (i) can only be made by assuming that the companion has giant dimensions (accretion disk?) but *does not* radiate like a black body in the optical. Part of the variations observed in the y band could then be caused either by the large companion contributing its own ellipsoidal variations [thus dropping assumption (b)] or by the companion eclipsing the red giant. This explanation seems however difficult to reconcile with the strong hints that the companion is a hot *compact* star provided by the IUE spectrum described by Schmid & Nussbaumer (1993). A radius of $\sim 9\ 10^{-2}$ R$_\odot$ is obtained for the companion from the black body approximation using the flux ratio at 550 nm derived above and adopting R = 40 R$_\odot$ and $T_{\rm eff}$ = 4300 K for the red giant.

Concerning possibility (ii), it is well known indeed that the location of the giant branch as predicted by stellar models is very sensitive to the model assumptions (particularly to the ratio of the mixing-length to the pressure scale height). There is no reason, however, to believe that the Geneva tracks are much in error since they have precisely been calibrated to match the observed giant branches of stellar clusters (Schaller et al. 1992). More-

over, dynamical solutions computed with $T_{\rm eff}$ at either boundary of the uncertainty range 4300±100 K applying to BD−21°3873 (Sect. 3 and Paper I) do not provide a better match to the evolutionary predictions.

Possibility (iii) seems to offer the best alternative, as several independent arguments indicate that BD−21°3873 is indeed tidally distorted by its companion, but with a Roche radius close to 40 $R_\odot$ to match the evolutionary tracks. First, $\log g$ = 1.25 is predicted for R = 37 $R_\odot$ and M = 0.9 $M_\odot$, in good agreement with the spectroscopically derived gravity $\log g$ = 1.0 (Sect. 3). A radius closer to the theoretical Roche radius ($R \sim R_{\rm R}$ = 90 $R_\odot$) would yield a much lower gravity of $\log g$ = 0.5, incompatible with the observed spectral features. Secondly, the very existence of the ellipsoidal variations implies that tidal effects efficiently distort the shape of the giant. Such tidal effects also synchronize the rotation with the orbital motion (e.g. Giuricin et al. 1984; Verbunt & Phinney 1995). A synchronous rotation velocity of $V \sin i \sim 6$ km s^{-1} is predicted for R = 37 $R_\odot$ and $\sin i$ = 0.87 [as derived from the mass function $f(M)$ and the assumption M_1 = 0.9 $M_\odot$ and M_2 = 0.45 $M_\odot$]. This is in good agreement with the upper limit $V \sin i \lesssim 6$ km s^{-1} estimated from the McDonald high-resolution spectra, and with $V \sin i = 5.4 \pm 0.7$ km s^{-1} obtained from CORAVEL (using the calibration of Benz & Mayor 1981), both derived assuming there is no contribution from macroturbulence. A radius close to 90 $R_\odot$ would lead instead to a synchronous rotation velocity of 14 km s^{-1}, much in excess of the observed values: such a large value would be easily detectable in both the McDonald spectra and the CORAVEL data.

A shrinkage of the Roche radius is in fact expected for luminous stars with high mass loss rates where some force drives the mass loss and reduces the effective gravity. That effect has been invoked as well in the context of X-ray binaries (Bolton 1975; Kondo et al. 1976). The existence of a force driving the mass loss will clearly modify the shape of the equipotential surfaces, as shown by Schuerman (1972). His Fig. 1 clearly shows that, when the more massive component is the source of this extra force as is the case here, the shape of the equipotential curves surrounding the giant star is not so much altered (so that the asymmetry needed to produce the ellipsoidal variations remains), though their size is significantly reduced.

In order to evaluate the magnitude of this effect in the case under study, the shape of the distorted giant star has been computed from the restricted three-body potential (Jacobi integral) in a rotating frame

$$\Phi = \frac{(1-\delta)\mu}{r_1} + \frac{(1-\mu)}{r_2} + \frac{x^2+y^2}{2} \qquad (2)$$

(where $\mu = M_1/(M_1+M_2)$, $r_1 = [(x+\mu-1)^2+y^2]^{1/2}$, $r_2 = [(x+\mu)^2+y^2]^{1/2}$), generalized to the case where an extra force $F_{\rm wind} = \delta(GM_1/r_1^2)$ drives the wind off the giant star. The center of mass of the binary system is at the origin of the adopted (x, y) coordinate set and the unit length corresponds to the separation of the components which are tied to the x axis.

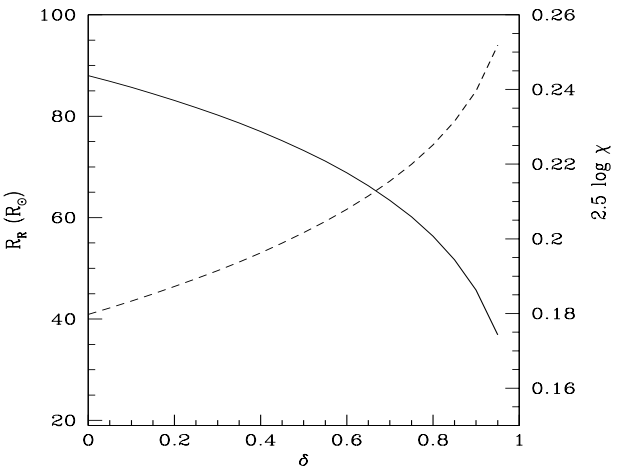

Fig. 10. The generalized Roche radius (solid line; left scale) and the asymmetry of the generalized Roche equipotential, expressed in a magnitude scale (dashed line; right scale), vs δ, the ratio of the force driving the mass loss of the giant to its gravity, for A = 200 $R_\odot$, M_1 = 0.9 $M_\odot$, M_2 = 0.45 $M_\odot$, $\mu = 2/3$, and P = 282 d

With these conventions, the more massive component is located at $(1-\mu, 0)$ and the less massive component at $(-\mu, 0)$. Conforming to the notations of Kopal (1959, Sect. III.3), let $(x_1, 0)$ be the coordinates of the inner Lagrangian point L_1 (or of its appropriate generalization when $\delta \neq 0$), where the potential takes the value $\Phi_1 = \Phi(x_1, 0)$, and let x_3 be such that $\Phi_1 = \Phi(x_3, 0)$, $x_3 \geq 1-\mu$. The asymmetry $\chi = |x_1 - x_3|/2y_5$ of the critical equipotential surrounding the more massive component and containing the inner Lagrangian point L_1 may then be computed as a function of δ by extracting y_5 (the maximum extension of the Φ_1 equipotential along y) from the system:

$$\begin{aligned} \Phi(x_5, y_5) &= \Phi_1 \\ \partial\Phi/\partial x(x_5, y_5) &= 0. \end{aligned} \qquad (3)$$

The transverse Roche radius $R_{\rm R} = y_5 A$ (where an orbital separation A = 200 $R_\odot$ has been adopted, corresponding to M_1 = 0.9 $M_\odot$, M_2 = 0.45 $M_\odot$ and P = 282 d) and the asymmetry, expressed as a magnitude ($2.5 \log \chi$), are presented on Fig. 10 for $\mu = 2/3$. As seen on that figure, the asymmetry χ slightly increases with δ, and so does the amplitude of the ellipticity effect for stars nearly filling their generalized Roche lobe. When $\delta = 0$ (i.e. in the absence of a force driving the mass loss), the Roche radius $y_5 A$ amounts to about 90 $R_\odot$, as indicated above. When δ approaches unity (i.e. the force driving the mass loss almost compensates the gravity of the mass-losing star), the Roche radius is considerably reduced, and when $\delta = 1$, the usual concept and usefulness of the Roche radius even vanish.

A generalized Roche radius of about 40 $R_\odot$, matching the evolutionary predictions for BD−21°3873 and triggering ellipsoidal variations as observed, can be obtained for δ close to unity. As argued by Kondo et al. (1976) and Theuns & Jorissen (1993), such a value for δ is not unexpected in view of the

fact that a red-giant wind appears to move out at nearly constant speed (except close to the photosphere), even before the point where it reaches the escape velocity, indicating that the net force on the wind is roughly zero (thus implying $\delta \sim 1$; see also Bowen 1988).

In conclusion, the present analysis of BD−21°3873 suggests that the usual Roche geometry may not be applicable in systems like symbiotic stars where the extra force driving the strong mass loss reduces the effective gravity (see Theuns & Jorissen 1993 and Theuns et al. 1996 for a three-dimensional hydrodynamical simulation revealing the intricacies of the gas flows in binary systems with parameters typical of symbiotic systems). A dynamical solution matching the evolutionary track of BD−21°3873 may be found provided that this extra force almost balances the gravity of the mass-losing star. Such a solution may appear somewhat *ad hoc*, though, since it required the introduction of the free parameter δ. A similar phenomenon has, however, been invoked in the context of X-ray binaries (Kondo et al. 1976 and references therein).

6. Conclusions

A detailed spectroscopic study of BD−21°3873 ($T_{\rm eff}$ = 4300 K, log g = 1.0, $M_{\rm bol} \sim -2.5$) has shown that it is a low-metallicity star ([Fe/H] = −1.3) with overabundances in the s-process elements. It is a twin of AG Dra studied in Paper I, another yellow symbiotic exhibiting the 'barium syndrome'. The s-process abundance distribution is best fitted by a single neutron exposure of τ = 1.2 mb^{-1}, and a neutron density log $N_{\rm n}$ = 8.3, as derived from the observed Rb/Zr ratio. These results confirm that the s-process synthesis is more efficient (larger τ and $N_{\rm n}$) at lower metallicities, a result already inferred from the study of barium and CH stars. That trend had been predicted by Clayton (1988) in the case that ^{13}C(α, n)^{16}O is the neutron source responsible for the operation of the s-process.

The barium syndrome seems to be shared by many yellow symbiotics (BD−21°3873, AG Dra, UKS-Ce1 and S32; see Schmid 1994), which also appear to be halo objects. This correlation may be a consequence of the fact that the barium syndrome is more easily produced at low metallicities. It is moreover argued that low-metallicity giants reach higher luminosities at a given $T_{\rm eff}$ than giants of lower metallicities, and thus suffer from a more severe mass loss making them appear as symbiotic stars.

The orbital parameters of BD−21°3873 have been derived from CORAVEL measurements, and are similar to those of barium stars. Like the other two yellow symbiotics with known periods (AG Dra and LT Del), the orbital period (282 d) of BD−21°3873 falls in the short-period tail of the distribution of barium stars. Periods for more yellow symbiotic stars are however required before one can conclude that this is a systematic effect.

The fact that BD−21°3873 exhibits ellipsoidal light variations has been used to narrow down the range of admissible parameters. However, no solution matching the Geneva evolutionary tracks could be found. This discrepancy has been interpreted as an indication that the usual Roche geometry is not applicable to systems where a strong mass loss from one component is driven by a force substantially reducing its effective gravity. This effect is also present in X-ray binaries, and makes the restricted three-body equipotentials around the (more massive) mass-losing component shrink. A solution matching the orbital parameters, the ellipsoidal lightcurve and the evolutionary constraints may be obtained when this effect is taken into account.

Acknowledgements. We thank M. Mayor and S. Udry for help with the CORAVEL data. The observers of the *Long-Term Photometry of Variables* project are gratefully acknowledged, as well as C. Sterken and J. Manfroid for their dedication to the LTPV project. Partial financial support for this project from the *Fonds National de la Recherche Scientifique* (Belgium) is acknowledged. KC acknowledges ON-CNPq for travel support. VVS acknowledges support from the National Science Foundation (AST93-14911) and the College of Science at UTEP.

References

Ake T.B., Johnson H.R., Ameen M.M., 1991, ApJ 383, 842
Allen D.A., 1980, MNRAS 192, 521
Allen D.A., 1984, Proc. Astron. Soc. Australia 5, 369
Anders E., Grevesse N., 1989, Geochim. Cosmochim. Acta 53, 197
Arkhipova V.P., Noskova R.I., 1985, Sov. Astron. Let. 11, 297
Arkhipova V.P., Noskova R.I., 1988, Sov. Astron. Let. 14, 188
Baranne A., Mayor M., Poncet J.L., 1979, Vistas in Astronomy 23, 279
Bell R.A., Eriksson K., Gustafsson B.E., Nordlund A., 1976, A&AS 23, 37
Benz W., Mayor M., 1981, A&A 93, 235
Biémont E., Grevesse N., Hannaford P., Lowe R.M., 1981, ApJ 248, 867
Biémont E., Karner C., Meyer G., Trager F., zu Putlitz G., 1982, A&A 107, 166
Blackwell D.E., Menom S.L.R., Petford A.D., 1983, MNRAS 204, 883
Blackwell D.E., Booth A.J., Haddock D.J., Petford A.D., Legget S.K., 1986, MNRAS 220, 549
Bolton C.T., 1975, ApJ 200, 269
Bowen G.H., 1988, ApJ, 329, 299
Brown J.A., Smith V.V., Lambert D.L., Dutchover E.Jr., Hinkle K.H., Johnson H.R., 1990, AJ 99, 1930
Charbonnel C., Meynet G., Maeder A., Schaerer D., 1996, A&AS 115, 339
Clayton D.D., 1988, MNRAS 234, 1
Drake J.J., Smith G., 1991, MNRAS 250, 89
Duquennoy A., Mayor M., Halbwachs J.L., 1991, A&AS 88, 281
Edvardsson B., Andersen J., Gustafsson B., Lambert D.L., Nissen P.E., Tomkin J., 1993, A&A 275, 101
Fuhr J.R., Martin G.A., Wiese W.L., 1988, J. Phys. Chem. Ref. Data 17, No. 4
Gilroy K.K., Sneden C., Pilachowski C.A., Cowan J.J., 1988, ApJ 327, 298
Giuricin G., Mardirossian F., Mezzetti M., 1984, A&A 141, 227
Hall D.S., 1990, AJ 100, 554
Hannaford P., Lowe R.M., Grevesse N., Biémont E., Whaling W., 1982, ApJ 261, 736
Iben I.Jr., Tutukov A.V., 1996, ApJS 105, 145
Jorissen A., 1989. In: H.R. Johnson & B. Zuckerman (eds.) Evolution of Peculiar Red Giant Stars (IAU Coll. 106). Cambridge University Press, p. 156

Jorissen A., 1997. In: J. Mikolajewska (ed.) Physical Processes in Symbiotic Binaries and Related Systems. Publ. N. Copernicus Foundation, Warsaw, in press
Jorissen A., Boffin H.M.J., 1992. In: Duquennoy A., Mayor M. (eds.) Binaries as Tracers of Stellar Formation. Cambridge Univ. Press, p. 110
Jorissen A., Hennen O., Mayor M., Bruch A., Sterken C., 1995, A&A 301, 707
Jorissen A., Schmitt J.H.M.M., Carquillat J.M., Ginestet N., Bickert K.F., 1996, A&A 306, 467
Jorissen A., Mowlavi N., Sterken C., Manfroid J., 1997, A&A, in press
Jorissen A., Van Eck S., 1997. In: R.F. Wing (ed.) The Carbon Star Phenomenon (IAU Symp. 177). Kluwer, Dordrecht, in press
Käppeler F., Beer H., Wisshak K., 1989, Rep. Prog. Phys. 52, 945
Kenyon S.J., 1988, AJ 96, 337
Kenyon S.J., 1994, Mem.Soc.Astron.It. 65, 135
Kenyon S.J., Garcia M.R., 1989, AJ 97, 194
Kolotilov E.A., Munari U., Yudin B.F., 1995, A&A 293, 815
Kondo Y., McCluskey G.E. Jr., Gulden S.L., 1976. In: Boldt E., Kondo Y. (eds.) X-ray Binaries. NASA-SP 389, Washington D.C., p. 499
Kopal Z., 1959. Close Binary Stars, Wiley, New York
Lambert D.L., Luck R.E., 1978, MNRAS 183, 79
Lambert D.L., Ries L.M., 1981, ApJ 248, 228
Lambert D.L., Heath J.E., Lemke M., Drake J.J., 1996, ApJS 103, 183
Lattanzio J.C., 1986, ApJ 311, 708
Lawler J.E., Dakin J.T., 1989, J. Opt. Sci. Am. B, 6, 1457
Luck R.E., Bond H.E., 1985, ApJ 292, 559
Lucy L.B., Sweeney M.A., 1971, AJ 76, 544
Magain P., 1989, A&A 209, 211
Malaney R.A., 1987, ApJ 321, 832
Malaney R.A., Lambert D.L., 1988, MNRAS 235, 695
Mayor M., Maurice E., 1985. In: Philip A.G.D., Latham D.W. (eds.) Stellar Radial Velocities (IAU Coll. 88). Davis press, p. 299
McCarthy J.K., Sandiford B.A., Boyd D., Booth J., 1993, PASP 105, 881
McClure R.D., 1984, PASP 96, 117
McClure R.D., Woodsworth A.W., 1990, ApJ 352, 709
McWilliam A., 1990, ApJS 74, 1075
Morris S.L., 1985, ApJ 295, 143
Morris S.L., Naftilan S.A., 1993, ApJ 419, 344
Munari U., 1989, A&A 208, 63
Munari U., Buson L.M., 1992, A&A 255, 158
Niehues M., Bruch A., Duerbeck H.W., 1992, The Messenger 67, 38
Olsen E.H., 1984, A&AS 57, 443
Proga D., Kenyon S.J., Raymond J.C., Mikolajewska J., 1996, ApJ 471, 930
Reimers D., 1975, Mem. Soc. Roy. Sci. Liège, 6th Ser., 8, 369
Schaller G., Schaerer D., Meynet G., Maeder A., 1992, A&AS 96, 269
Schild H., Mürset U., Schmutz W., 1996, A&A 306, 477
Schmid H.M., 1989, A&A 211, L31
Schmid H.M., 1994, A&A 284, 156
Schmid H.M., Nussbaumer H., 1993, A&A 268, 159
Schuerman D.W., 1972, Ap&SS 19, 351
Schulte-Ladbeck R.E., 1988, A&A 189, 97
Smith, G., Edvardsson B., Frisk, U., 1986, A&A 165, 126
Smith V.V., Lambert D.L., 1984, PASP 96, 226
Smith V.V., Lambert D.L., 1990, ApJS 72, 387
Smith V.V., Cunha, K., Jorissen, A. & Boffin, H., 1996, A&A 315, 179 (Paper I)
Sneden C., 1973, ApJ 184, 839
Sterken C., 1983, The Messenger 33, 10
Sterken C., Manfroid J., Beele D., de Koff S., Eggenkamp I.M.M.G., Göcking K., Jorissen A., Kaufer A., Kuss C., Schoenmakers A.P., Stil J.M., van Loon J., Vink J., Vrielmann S., Wälde E., 1995a. Fourth Catalogue of Stars measured in the Long-Term Photometry of Variables Project (1992 – 1994). European Southern Observatory, Scientific Report 16
Sterken C., Manfroid J., Beele D., de Koff S., Eggenkamp I.M.M.G., Göcking K., Jorissen A., Kaufer A., Kuss C., Schoenmakers A.P., Stil J.M., van Loon J., Vink J., Vrielmann S., Wälde E., 1995b, A&AS 113, 31
Straizys V., Kurilienė G., 1975, Bull. Vilnius Obs. 42, 31
Theuns T., Jorissen A., 1993, MNRAS 265, 946
Theuns T., Boffin H.M.J., Jorissen A., 1996, MNRAS 280, 1264
Tomkin J., Lambert D.L., 1983, ApJ 273, 722
Tomkin J., Lambert D.L., 1986, ApJ 311, 819
Vanture A.D., 1992a, AJ 104, 1997
Vanture A.D., 1992b, AJ 103, 2035
Wheeler J.G., Sneden C., Truran J.W., 1989, ARA&A 27, 279
Wiese W.L., Martin G.A., 1980, NSDRS-NBS, 68
Wilson R.E., Devinney E.J., 1971, ApJ 166, 605
Woolf V.M., Tomkin J., Lambert D.L., 1995, ApJ 453, 660
Youssef N.M., Amer M.A., 1989, A&A 220, 281
Zhao G., Magain P., 1991, A&A 244, 425

This article was processed by the author using Springer-Verlag LaTeX A&A style file *L-AA* version 3.